

# Towards AC Feasibility of DCOPF Dispatch

Michael A. Boateng\*, Russell Bent†, Sidhant Misra†, Parikshit Pareek‡, Pascal Van Hentenryck\*, Daniel Molzahn\*

\* School of Electrical and Computer Engineering, Georgia Institute of Technology

Atlanta, Georgia, USA, {mboateng6, pvh, molzahn}@gatech.edu

† T5: Applied Mathematics and Plasma Physics, Los Alamos National Laboratory

Los Alamos, New Mexico, USA, {rbent, sidhant}@lanl.gov

‡ Department of Electrical Engineering, Indian Institute of Technology Roorkee, India, pareek@ee.iitr.ac.in

**Abstract**—DC Optimal Power Flow (DCOPF) is widely utilized in power system operations due to its simplicity and computational efficiency. However, its lossless, reactive power-agnostic model often yields dispatches that are infeasible under practical operating scenarios such as the nonlinear AC power flow (ACPF) equations. While theoretical analysis demonstrates that DCOPF solutions are inherently AC-infeasible, their widespread industry adoption suggests substantial practical utility. This paper develops a unified DCOPF → ACPF pipeline to recover AC feasible solutions from DCOPF-based dispatches. The pipeline uses four DCOPF variants and applies AC feasibility recovery using both distributed slack allocation and PV/PQ switching. The main objective is to identify the most effective pipeline for restoring AC feasibility. Evaluation across over 10,000 dispatch scenarios on various test cases demonstrates that the structured ACPF model yields solutions that satisfy both the ACPF equations, and all engineering inequality constraints. In a 13,659-bus case, the mean absolute error and cost differences between DCOPF and ACOPF are reduced by 75% and 93%, respectively, compared to conventional single slack bus methods. Under extreme loading conditions, the pipeline reduces inequality constraint violations by a factor of 3 to 5.

**Index Terms**—AC Feasibility, DC Power Flow (DCPF), Distributed Slack, Loss-Augmented DCOPF, Newton Method.

## NOMENCLATURE

$\mathcal{N}$	Set of buses; $\mathcal{N} = \{1, \dots, N\}$
$\mathcal{E}$	Set of lines {lines run from $i \rightarrow j$ or $j \rightarrow i$ }
$\mathcal{G}, \mathcal{L}$	Set of generators and loads $\{\mathcal{G}, \mathcal{L} \subseteq \mathcal{N}\}$
$r, b, g$	Line resistance, susceptance, and conductance
$\mathbf{Y}$	Complex branch line admittance
$\Phi$	Line-Bus PTDF matrix, size $\mathcal{E} \times \mathcal{N}$
$s_{tx}^{\max}$	Apparent power transformer limit
$i_{line}^{\max}$	Current flow line limit
$p_g^{\min}, p_g^{\max}$	Active power generation limits
$\mathbf{p}_g, \mathbf{q}_g$	Active and reactive power generation
$s_g$	Complex power generation; $\mathbf{p}_g + \mathbf{j} \cdot \mathbf{q}_g$
$\mathbf{p}_d, \mathbf{q}_d$	Active and reactive power demand
$q_g^{\min}, q_g^{\max}$	Reactive power generation limits
$v_i^{\min}, v_i^{\max}$	Voltage magnitude limits, for $v_i$
$\theta^{dc}, \theta^{ac}$	Voltage angles from DC and AC models
$\pi_g$	Slack participation factor for generators
$\ell^{\text{tot}}, \epsilon$	Total losses across network, tolerance

The work was partially funded by Los Alamos National Laboratory's Directed Research and Development project, "Artificial Intelligence for Mission (ArtIMis)" under U.S. DOE Contract No. DE-AC52-06NA25396.

Submitted to the 24th Power Systems Computation Conference (PSCC 2026).

## I. INTRODUCTION

The linearity of the DC power flow equations provides the DC Optimal Power Flow (DCOPF) problem with significant computational advantages over the AC Optimal Power Flow (ACOPF) problem [1]. These advantages come at the cost of accuracy relative to ACOPF solutions. Since inaccuracies in DCOPF solutions can lead to suboptimal operation and violations of operational limits, studying DC power flow accuracy is a long-running research topic that includes both empirical and analytical assessments. For instance, [1]–[10] empirically study DC power flow accuracy for various applications. Analytical analyses, e.g., [11]–[13], rigorously bound the worst-case DCPF approximation error, but these bounds are not necessarily indicative of typical accuracy.

Of particular relevance to this paper, Baker in [14] analytically proved that, under nonzero loading conditions in networks with positive resistances and reactances, the feasible regions of DCOPF and ACOPF are disjoint. This implies that the optima of conventional DCOPF problems are never AC feasible, i.e., never satisfy the AC power flow equations. The primary argument in [14] relates to the difference in losses between the DC and AC power flow equations. Baker further shows that even DCOPF variants which incorporate loss-adjustment mechanisms will still fail to provide AC feasible solutions due to a similar argument at the level of individual buses.

The theory in [14] provides an important foundational result regarding the accuracy of DC power flow approximations. However, this theory does not address how frequently the solutions to DCOPF problems can be *easily restored* to acceptable AC feasible operating points, i.e., operating points which satisfy both the AC power flow equations and the limits on generator outputs, voltage magnitudes, and line flows. This paper empirically addresses this question. Solving the AC power flow equations is a natural approach for restoring an AC feasible operating point from a solution to a DCOPF problem. By fixing the generators' active power setpoints to those from the DCOPF solution and the voltage magnitudes to a nominal value such as 1 per unit, one can easily construct a system of AC power flow equations that are frequently solvable via standard Newton-Raphson methods. The resulting power flow solution is feasible with respect to the AC power flow equations by construction. If the power flow solution satisfies limits on generator outputs, voltage magnitudes, and line flow limits, it is

a feasible operating point with respect to the ACOPF problem's constraints. Thus, while the DCOPF problem's solution is not itself AC feasible as shown in [14], it may be the case that an AC feasible solution can often be easily obtained.

Indeed, much of the prior literature on DC power flow accuracy (e.g., [1]–[10]) and restoration of AC feasible solutions (e.g., [15]–[19]) takes this AC power flow approach. However, while existing work performs extensive numerical studies on this topic, there are key gaps in the existing literature. Namely, prior research either 1) focuses on simplistic ACPF models that use a single slack bus or neglect the generators' reactive power limits *and/or* 2) focuses on DC power flow accuracy over a range of power injections as opposed to the solutions to DCOPF problems. Since DCOPF solutions are usually extreme points in the operating region, approximation accuracy at these points is not necessarily aligned with DC power flow accuracy over the entire operating region. To the best of our knowledge, the only other paper that simultaneously considers distributed slack and reactive power limited formulations for ACPF settings similar to ours is [17]. The paper examined reactive power control in ACPF, and addressed a slack distribution formulation – though independently, and only applies distributed slack on a 23-bus system. Further, it does not apply any of the formulations in the context of feasibility restoration for DCOPF solutions.

This work addresses these gaps using a “structured” ACPF model that more accurately represent generator behavior via distributed slack bus and PV/PQ switching models by imposing realistic generator limits on both active and reactive power outputs. Using the structured ACPF model with several DCOPF approximation variants, results from the DCOPF → ACPF pipeline—solving a DCOPF and evaluating the resulting setpoints with an ACPF—demonstrate that different DCOPF formulations influence DCOPF dispatch outcomes and the ability to recover AC feasibility with respect to the ACOPF constraints. This provides an important empirical counterpart to the theoretical findings of [14] on the *ease of restoration* for DCOPF solutions. In summary, the paper's contributions are:

- A DCOPF → ACPF recovery pipeline identifying the most effective DC formulation for obtaining AC feasible solutions across a variety of large-scale power systems.
- An assessment of the impacts of ACPF variants—featuring distributed slack and/or PV/PQ switching models—in the context of AC-feasibility restoration.
- A systematic sensitivity analysis of the pipeline to load perturbations and guidance on its importance for improving feasibility-restoration workflows.

The paper is organized as follows. Section II introduces the pipeline with (A) loss-augmented DCOPF models, and (B) a structured ACPF formulation. Section III shows the numerical results, and Section IV concludes with future directions.

## II. METHODOLOGY

To investigate the most effective DCOPF → ACPF pipeline as shown in Fig. 1, two components were integrated: (i) a *loss-aware* DCOPF embedding a loss approximation while remaining convex and efficient, and (ii) a *structured* ACPF

### Model 1: DC Optimal Power Flow (DCOPF) Formulation

$$\min \sum_{i \in \mathcal{G}} (c_{2i} p_{gi}^2 + c_{1i} p_{gi} + c_{0i}) \quad (\text{Cost Minimization}) \quad (1a)$$

$$\text{s.t. } p_{gi} - p_{di} = \sum_{j \in \mathcal{E}} \vec{p}_{ji} - \sum_{j \in \mathcal{E}} \vec{p}_{ij} \quad \forall i \in \mathcal{N} \quad (\text{Power Balance}) \quad (1b)$$

$$\vec{p}_{ij} = b_{ij}(\theta_i^{\text{dc}} - \theta_j^{\text{dc}}) \quad \forall (i, j) \in \mathcal{E} \quad (\text{DC Flow}) \quad (1c)$$

$$|\vec{p}_{ij}| \leq p_{ij}^{\max} \quad \forall (i, j) \in \mathcal{E} \quad (\text{Line Limit}) \quad (1d)$$

$$p_g^{\min} \leq p_g \leq p_g^{\max} \quad (\text{Gen. Active Power}) \quad (1e)$$

- Different inputs to DCOPF and ACPF variants
- Various DCOPF and ACPF formulations can be paired together
- Recorded inequality constraint violations to observe ACOPF feasibility

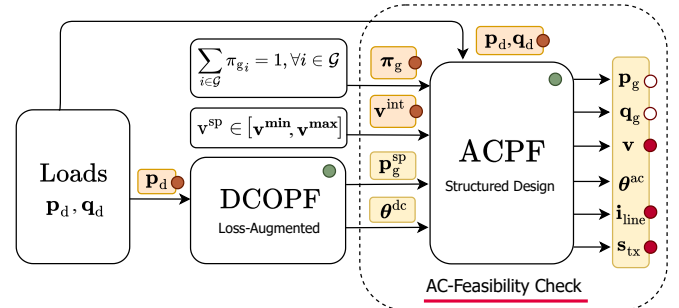


Fig. 1: Pipeline of the DCOPF → ACPF model. The DCOPF gives  $p_g^{\text{sp}}$  and  $\theta^{\text{dc}}$  from input  $p_d$ . The ACPF performs feasibility checks with distributed slack using participation factors ( $\pi_g$ ). Voltage initialization ( $v^{\text{int}}$ ) aids in convergence. ACOPF constraints are marked with red.

with distributed slack and PV/PQ switching. The stages are coupled: the DCOPF provides generator setpoints, and the ACPF applies minimal adjustments to obtain solutions that are nearly or fully AC feasible — i.e., solutions that satisfy both the ACPF equations and the full ACOPF inequality constraints.

### A. DCOPF with Line Loss Approximation

To improve the accuracy of the DCOPF while preserving tractability, several loss-augmented DCOPF variants have been developed in the literature, three of which are described next.

1) *Linear Line Loss Factor Model (LLLF)* [16], [20]: Using the DC PTDF ( $\Phi$ ) matrix from the DC power flow approximation [21], resistive losses are linearized about a reference DC operating point. Total losses are expressed as:

$$\ell^{\text{tot}} = \ell^{\text{ref}} + \boldsymbol{\lambda}^\top \mathbf{p}, \quad (2)$$

where  $\ell^{\text{ref}}$  is a scalar offset,  $\boldsymbol{\lambda}$  is the (linear) loss-factor vector, and  $\mathbf{p}$  stacks bus active-power injections. The loss factors follow from differentiating the approximate quadratic loss  $\sum_{(i,j)} r_{ij} \vec{p}_{ij}^2$  via the chain rule, yielding  $\boldsymbol{\lambda}^\top = -2(\mathbf{R} \odot \vec{\mathbf{p}}^{\text{ref}})^\top \boldsymbol{\Phi}$ , and the offset is chosen to match the true loss at the reference,  $\ell^{\text{ref}} = -\boldsymbol{\lambda}^\top \mathbf{p}^{\text{ref}} + \sum_{(i,j) \in \mathcal{E}} r_{ij} (\vec{p}_{ij}^{\text{ref}})^2$ . Here,  $\mathbf{R}$  stacks line resistances  $r_{ij}$ ,  $\vec{\mathbf{p}}^{\text{ref}}$  are oriented reference branch flows, and  $\odot$  denotes the Hadamard product [21].

2) *Line Loss Quadratic Convex Program (LQCP)* [16]: This model incorporates line losses directly through convex quadratic constraints. Power balance and operational limits

follow (1d)–(1e). Flows are modeled as being linear in voltage angles via (1c). For each line  $(i, j)$ , losses are modeled as:

$$\vec{p}_{ij} + \vec{\hat{p}}_{ij} \geq r_{ij} (\vec{p}_{ij})^2. \quad (3)$$

While this formulation is convex, the presence of nonlinear constraints may increase computational burden [16].

3) *Line Loss Outer Approximation (LLOA)* [16]: This approach approximates the nonlinear LQCP loss constraints using supporting hyperplanes. For a given reference flow  $\vec{p}_{ij}^{\text{ref}}$ , the quadratic loss term is outer-approximated linearly via:

$$\vec{p}_{ij} + \vec{\hat{p}}_{ij} \geq r_{ij} \left[ -(\vec{p}_{ij}^{\text{ref}})^2 + 2\vec{p}_{ij}^{\text{ref}} \cdot \vec{p}_{ij} \right], \quad (4)$$

which makes the approximation conservative with respect to the LQCP formulation. The total losses  $\sum_{(i,j)} \ell_{ij}$  are embedded into the system power balance via  $\sum_i p_i = \sum_d p_d + \sum_{(i,j)} \ell_{ij}$ , with each  $\ell_{ij}$  lower-bounded by its linear approximation. The LLOA approach allows fast, warm-started dispatch [16].

### B. Structured AC Power Flow Model

Following the DCOPF, a structured ACPF is solved via the Newton–Raphson method, with a distributed slack to allocate active-power imbalances across generators and PV/PQ switching to handle reactive-power limits. For a comprehensive pipeline analysis, a total of four AC variants are utilized.

1) *Distributed Slack Model*: A conventional ACPF assigns all active-power imbalance to a single slack generator, often producing unrealistic dispatch and voltage bias. To address this, a *headroom-based* distributed slack formulation is used, sharing the total mismatch  $\ell^{\text{tot}}$ —the signed active-power deficit or surplus between the DCOPF setpoints  $p_{gi}^{\text{sp}}$ , and the current AC state  $(\theta, \mathbf{V})$ —across generators in proportion to their available headroom (i.e., margin to their upper active power output limit). This adaptive allocation prevents infeasible loading during AC feasibility recovery, unlike equal or maximum-capacity participation schemes that disregard operating limits. As shown in Model 2, (5a) defines each generator’s headroom  $h_i$  as the upward margin to the active-power limit; generators at their upper limits have  $h_i = 0$  and thus do not absorb further deficit. The participation factor  $\pi_{gi}$  defined in (5b) allocates a fraction of  $\ell^{\text{tot}}$  to each unit, and a capacity-proportional fallback ensures feasibility when  $\sum_i h_i = 0$ . Updated injections follow (5c), with  $\pi_{gi}$  recomputed and normalized at each Newton–Raphson iteration to maintain  $\pi_{gi} \geq 0$  and  $\sum_i \pi_{gi} = 1$ . This weighting preserves realism under load perturbations, enhances numerical stability, and improves cost allocation accuracy [22].

2) *Reactive Power Control*: The ACPF also utilizes a reactive power control mechanism via bus-type switching—a standard method for representing generator behavior in power flow analysis. As shown in Fig. 2, the bus transitions between  $\mathbf{PQ}^{\max}$ ,  $\mathbf{PV}$ , and  $\mathbf{PQ}^{\min}$  states based on  $(q_{gi}, v_i^{\text{sp}})$ . In practice, most solvers apply small tolerances to avoid oscillatory switching during Newton–Raphson iterations. Accordingly, a deadband  $(\epsilon_q, \epsilon_v)$  is imposed such that  $|q_g - q_g^{\text{lim}}| \leq \epsilon_q$  and  $|v^* - v^{\text{sp}}| \leq \epsilon_v$ , preventing transitions within this range. When reactive power violations exceed  $\epsilon_q$ ,  $\mathbf{PV}$  buses switch to  $\mathbf{PQ}$ , clamping reactive power at its bound. Reversion occurs only

### Model 2: Headroom-Based Slack Distribution

$$h_i = \max(p_{gi}^{\max} - p_{gi}^{\text{sp}}, 0), \quad \forall i \in \mathcal{G} \text{ (Headroom)} \quad (5a)$$

$$\pi_{gi} = \begin{cases} \frac{h_i}{\sum_{i \in \mathcal{G}} h_i}, & \text{if } \sum_{i \in \mathcal{G}} h_i > 0, \\ \frac{p_{gi}^{\max}}{\sum_{i \in \mathcal{G}} p_{gi}^{\max}}, & \text{otherwise,} \end{cases} \quad \forall i \in \mathcal{G} \text{ (Slack share)} \quad (5b)$$

$$p_{gi} = p_{gi}^{\text{sp}} + \pi_{gi} \ell^{\text{tot}}, \quad \forall i \in \mathcal{G} \text{ (New dispatch)} \quad (5c)$$

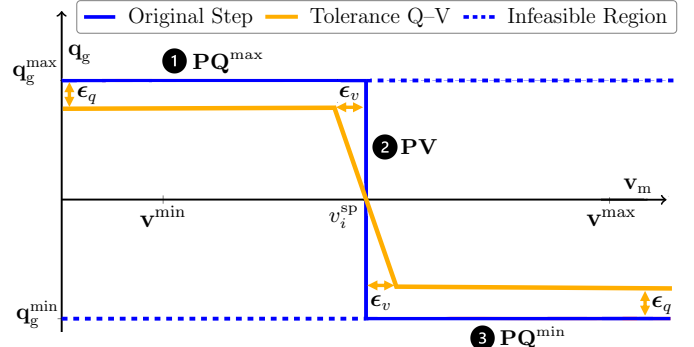


Fig. 2: The generator bus-type switching logic. The **blue curve** is the discrete logic. The bus transitions between  $\mathbf{PQ}^{\max}$ ,  $\mathbf{PV}$ , and  $\mathbf{PQ}^{\min}$  states, based on  $q_{gi}$  and  $v_i^{\text{sp}}$ . The **blue dashed lines** are infeasible regions where the generator cannot maintain voltage control while obeying reactive power limits. The **orange curve** is the tolerance-based control, with tolerances  $\epsilon_q$  and  $\epsilon_v$  on reactive power and voltage.

when voltages move beyond  $\epsilon_v$ . This practical scheme limits switching per Newton solve, enforces reactive power feasibility, and improves convergence by reducing oscillations. Although it does not guarantee voltage-limit satisfaction, it maintains feasible reactive injections and numerically stable operation.

Unstable and erratic iterations from discrete PV/PQ switching noted in prior studies [23], [24] were rarely observed in AC<sub>SPF</sub>, and while homotopy-based methods [17] can further reduce iterations, the tolerance-based deadband offers sufficient robustness and integrates seamlessly with the ACPF framework.

In Newton-Raphson ACPF, *total iteration count* records all inner iterations needed for convergence under fixed bus types, while the *PV/PQ switching count* tracks outer iterations where generator buses change type as reactive limits are enforced or released. Both iteration counts are recorded in Section III.

For the sake of notational brevity, the paper hereafter denote four ACPF variants as follows: AC<sub>BASE</sub> uses a single slack bus with no generator control, AC<sub>BTS</sub> applies discrete PV/PQ switching (blue curve in Fig. 2), AC<sub>DS</sub> employs distributed slack control only, and AC<sub>SPF</sub> (Structured Power Flow) combines headroom-based distributed slack (Model 2) with tolerance-based PV/PQ switching (orange curve in Fig. 2).

## III. NUMERICAL EXPERIMENTS

The various combinations of DCOPFs and ACPFs described in Section II were evaluated on a diverse suite of MATPOWER 8.1 test cases [25]. This includes IEEE cases {ieee\_30, ieee\_ne\_39, ieee\_118}, ACTIVSg grids {South\_Carolina\_500, Texas\_2000}, PEGASE networks {pegase\_89, pegase\_1354, pegase\_2869},

TABLE I: NUMBER OF VIOLATIONS IN BASE CASE FOR DCOPF → ACPF PIPELINES USING STANDARD TEST CASES

Test case	AC type	Active Power Violations				Reactive Power Violations				Voltage Violations				Thermal Violations			
		DC <sub>BASE</sub>	DC <sub>LLLF</sub>	DC <sub>LQCP</sub>	DC <sub>LLOA</sub>	DC <sub>BASE</sub>	DC <sub>LLLF</sub>	DC <sub>LQCP</sub>	DC <sub>LLOA</sub>	DC <sub>BASE</sub>	DC <sub>LLLF</sub>	DC <sub>LQCP</sub>	DC <sub>LLOA</sub>	DC <sub>BASE</sub>	DC <sub>LLLF</sub>	DC <sub>LQCP</sub>	DC <sub>LLOA</sub>
case_118	AC <sub>BASE</sub>	1	1	0	1	22	21	18	16	0	1	0	0	0	0	0	0
	AC <sub>BTS</sub>	1	1	0	1	0	0	0	0	1	0	0	1	1	1	1	1
	AC <sub>DS</sub>	0	0	0	0	19	20	25	26	0	1	0	0	0	0	0	0
	AC <sub>SPF</sub>	0	0	0	0	0	0	0	0	0	1	0	0	0	0	0	0
case_1354	AC <sub>BASE</sub>	1	1	1	1	91	70	85	76	2	1	1	1	3	17	5	11
	AC <sub>BTS</sub>	1	1	0	1	0	0	0	0	1	1	1	1	6	13	5	10
	AC <sub>DS</sub>	0	0	0	0	82	67	87	89	1	1	1	0	5	15	1	4
	AC <sub>SPF</sub>	0	0	0	0	0	0	0	0	0	1	1	0	0	13	2	0
case_2869	AC <sub>BASE</sub>	1	1	1	1	310	190	87	115	2	1	1	1	12	4	3	16
	AC <sub>BTS</sub>	1	1	1	1	0	0	0	0	14	7	4	2	12	25	13	22
	AC <sub>DS</sub>	0	0	0	0	365	213	164	96	2	2	3	0	18	17	5	11
	AC <sub>SPF</sub>	0	0	0	0	0	0	0	0	0	1	0	0	6	1	0	0
case_13659	AC <sub>BASE</sub>	1	1	1	0	1215	1028	971	1012	19	6	6	5	68	65	62	62
	AC <sub>BTS</sub>	1	1	0	1	0	0	0	0	213	170	69	62	93	55	52	60
	AC <sub>DS</sub>	0	0	0	0	1003	980	956	940	22	16	17	16	40	42	32	33
	AC <sub>SPF</sub>	0	0	0	0	0	0	0	0	0	7	0	3	0	24	0	21

TABLE II: MAXIMUM VIOLATION VALUE IN BASE CASE FOR DCOPF → ACPF PIPELINES USING STANDARD TEST CASES

Test case	AC type	Active Power Violations (p.u.)				Reactive Power Violations (p.u.)				Voltage Violations (p.u.)				Thermal Violations (%)				
		DC <sub>BASE</sub>	DC <sub>LLLF</sub>	DC <sub>LQCP</sub>	DC <sub>LLOA</sub>	DC <sub>BASE</sub>	DC <sub>LLLF</sub>	DC <sub>LQCP</sub>	DC <sub>LLOA</sub>	DC <sub>BASE</sub>	DC <sub>LLLF</sub>	DC <sub>LQCP</sub>	DC <sub>LLOA</sub>	DC <sub>BASE</sub>	DC <sub>LLLF</sub>	DC <sub>LQCP</sub>	DC <sub>LLOA</sub>	
case_118	AC <sub>BASE</sub>	0.002	0.001	0.000	0.001	1.538	1.528	1.489	1.469	0.000	0.010	0.000	0.000	0.000	0.000	0.000	0.000	0.000
	AC <sub>BTS</sub>	0.001	0.001	0.000	0.001	0.000	0.000	0.000	0.000	0.008	0.005	0.000	0.000	4.472	4.470	4.100	4.001	
	AC <sub>DS</sub>	0.000	0.000	0.000	0.000	1.234	1.202	1.113	1.110	0.000	0.020	0.000	0.000	0.000	0.000	0.000	0.000	0.000
	AC <sub>SPF</sub>	0.000	0.000	0.000	0.000	0.000	0.000	0.000	0.000	0.000	0.000	0.000	0.000	0.000	0.000	0.000	0.000	0.000
case_1354	AC <sub>BASE</sub>	0.024	0.016	0.012	0.012	14.29	15.78	13.72	13.88	0.030	0.024	0.016	0.009	14.16	12.59	11.73	11.83	
	AC <sub>BTS</sub>	0.014	0.013	0.000	0.014	0.000	0.000	0.000	0.000	0.017	0.015	0.014	0.012	18.85	16.60	17.14	19.07	
	AC <sub>DS</sub>	0.000	0.000	0.000	0.000	12.78	12.35	12.10	12.12	0.021	0.016	0.011	0.000	15.42	11.23	8.433	9.761	
	AC <sub>SPF</sub>	0.000	0.000	0.000	0.000	0.000	0.000	0.000	0.000	0.000	0.020	0.010	0.000	0.000	15.65	3.810	0.000	0.000
case_2869	AC <sub>BASE</sub>	2.522	1.714	1.131	1.362	14.51	14.62	14.08	14.53	0.026	0.020	0.021	0.024	27.56	17.42	12.53	11.67	
	AC <sub>BTS</sub>	2.121	1.032	2.116	1.089	0.000	0.000	0.000	0.000	0.039	0.027	0.023	0.025	24.37	19.62	14.09	20.96	
	AC <sub>DS</sub>	0.000	0.000	0.000	0.000	16.02	14.39	11.76	11.76	0.033	0.020	0.017	0.002	26.78	14.34	9.051	9.803	
	AC <sub>SPF</sub>	0.000	0.000	0.000	0.000	0.000	0.000	0.000	0.000	0.024	0.000	0.000	0.000	6.732	4.329	0.000	0.000	
case_13659	AC <sub>BASE</sub>	43.10	42.05	44.30	0.000	8.790	7.322	6.999	6.704	0.063	0.055	0.053	0.042	55.45	56.01	48.67	46.34	
	AC <sub>BTS</sub>	44.52	43.46	0.000	33.80	0.000	0.000	0.000	0.000	0.129	0.112	0.122	0.122	75.43	70.13	62.24	67.60	
	AC <sub>DS</sub>	0.000	0.000	0.000	0.000	9.334	7.592	6.178	6.207	0.071	0.067	0.066	0.061	46.73	41.28	40.01	40.13	
	AC <sub>SPF</sub>	0.000	0.000	0.000	0.000	0.000	0.000	0.000	0.000	0.008	0.000	0.007	0.000	15.65	0.000	0.000	13.81	

pegase\_9241, pegase\_13659}, and a large-scale RTE case {rte\_6468}. Computations were carried out on the Darwin high-performance computing system at Los Alamos National Laboratory. Experiments used a single 24-core compute node equipped with 32 GB of RAM. The ACOPFs and DCOPFs variants were solved using `PowerModels.jl` [26]. The design and implementation of the custom ACPF was formulated using `pandapower.py` [27]. Active power demands ( $\mathbf{p}_d$ ) at load buses were perturbed using Gaussian multiplicative noise, where each positive demand was scaled by  $\xi \sim \mathcal{N}(1.0, \sigma^2)$  with  $\sigma \in (5\%, 15\%)$ . Reactive power ( $\mathbf{q}_d$ ) was recomputed from randomly sampled power factors in  $[0.95, 1.0]$ , and 1000 samples were evaluated per testcase. Since distributed slack and bus-type switching can change the Jacobian's structure across iterations, we rebuild the sparse system when the active set changes while exploiting sparsity at each step. These optimizations yield a scalable Newton-Raphson solver. The solver tolerance was set to  $10^{-6}$  p.u., while the tolerances for reactive power control were  $10^{-4}$  p.u. for  $\epsilon_q$  (reactive power) and  $10^{-5}$  p.u. for  $\epsilon_v$  (voltage). All results reported correspond to samples that converged. The mean absolute error (MAE) and percent cost difference (CD) are computed as follows:

$$\text{MAE} = \frac{1}{G} \|\mathbf{p}_g^{\text{DC} \rightarrow \text{AC}} - \mathbf{p}_g^{\mathcal{O}}\|_1, \quad (6)$$

$$\text{CD} = \frac{|\text{Cost}^{\text{DC} \rightarrow \text{AC}} - \text{Cost}^{\mathcal{O}}|}{\text{Cost}^{\mathcal{O}}} \cdot 100, \quad (7)$$

where  $G$  is the number of generators,  $\mathbf{p}_g^{\text{DC} \rightarrow \text{AC}}$  is the generation vector after the DCOPF → ACPF pipeline, and  $\mathbf{p}_g^{\mathcal{O}}$  is the ACOPF-based reference used as a ground truth.

#### A. ACOPF Feasibility Study with DCOPF → ACPF Variants

This section evaluates violations of the ACOPF constraints in Fig. 1 across the different DCOPF → ACPF pipelines. Tables and charts summarize these violations and their reduction factors under loss-augmented DCOPFs and the ACPF variants.

1) *Violation Tables Analysis*: Tables I and II show that the distributed-slack reconciliation AC<sub>SPF</sub> delivers the fewest violations across all DC initializations and systems. In case\_13659, reactive-power violations are noticeably high for AC<sub>BASE</sub> and AC<sub>DS</sub>, since these lack reactive control. The counts are 1215/1028/971/1012 for AC<sub>BASE</sub> across DC<sub>BASE</sub>/DC<sub>LLLF</sub>/DC<sub>LQCP</sub>/DC<sub>LLOA</sub>, and 1003/980/956/940 for AC<sub>DS</sub>. By contrast, both AC<sub>BTS</sub> and AC<sub>SPF</sub> keep reactive violations at zero, with AC<sub>SPF</sub> also maintaining voltage violations low (0/7/0/3) and thermal violations modest (0/24/0/21). For active-power violations, the distributed slack in AC<sub>DS</sub> and AC<sub>SPF</sub> again drives violations to zero across all DC variants. However, AC<sub>BASE</sub> and AC<sub>BTS</sub> struggle: in case\_13659, maximum per-unit active-power violations reach 43.10/42.05/44.30/0.000 p.u. under AC<sub>BASE</sub> and 44.52/43.46/0.000/33.80 p.u. under AC<sub>BTS</sub>. For AC<sub>SPF</sub>, maximum active- and reactive-power violations remain 0.000 p.u. in every case and DC variant. Thus, AC<sub>SPF</sub> combines the best of both worlds, eliminating active and reactive violations. AC<sub>SPF</sub> also seems to restore feasibility for DC<sub>BASE</sub> consistently. This will be revisited in the sensitivity analysis, later in this section.

Looking horizontally within any fixed AC reconciliation, violations generally fall as we move from the lossless DC<sub>BASE</sub> to the lossy DC<sub>LQCP</sub>/DC<sub>LLOA</sub>. DC<sub>LLLF</sub> usually improves on DC<sub>BASE</sub> but less reliably. As summarized in Section II, the

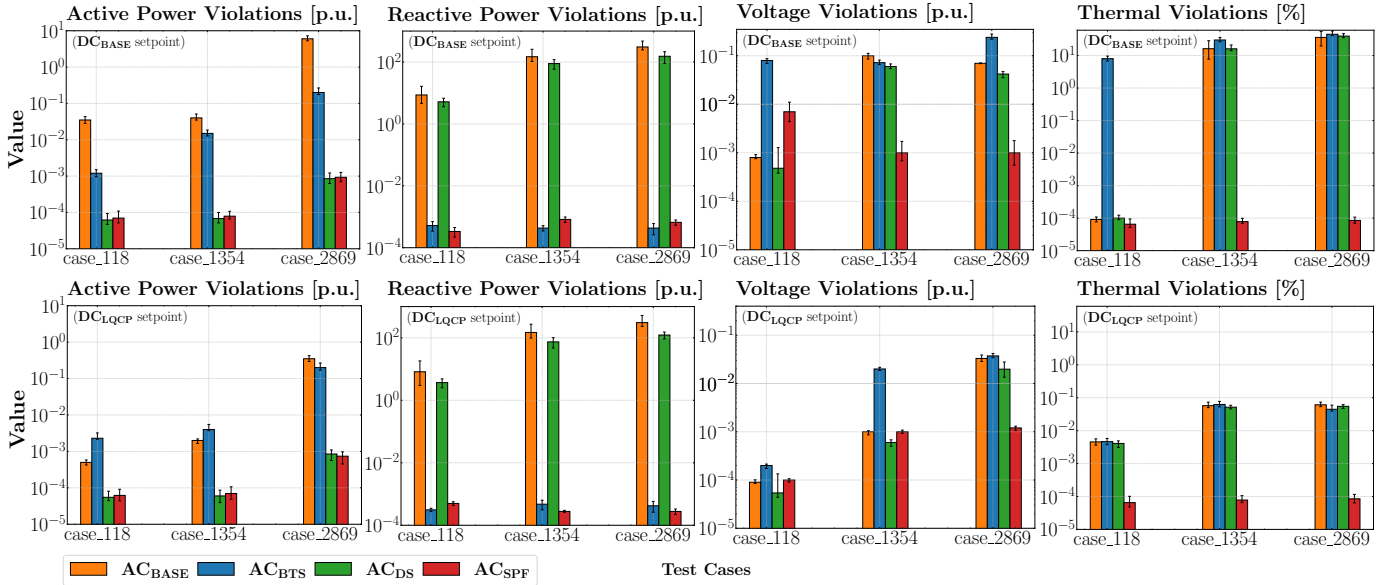


Fig. 3: Comparison of the sum total of violations in different AC power flow formulations across various cases: `case_118`, `case_1354`, and `case_2869` (with mean and min-max error bars). The pipelines shown have different DC setpoints: (top)  $DC_{BASE}$  and (bottom)  $DC_{LQCP}$ . The plots are taken over load uncertainty with  $\sigma = 15\%$ , for 1000 samples per case. Shown are the active power, reactive power, voltage, and thermal violations, with y-axes on log-scales. Results are reported for  $AC_{BASE}$  (orange),  $AC_{BTS}$  (blue),  $AC_{DS}$  (green), and  $AC_{SPF}$  (red).

superior accuracy of  $DC_{LQCP}$  and  $DC_{LLOA}$  arises because they include lossy formulations that more faithfully capture  $I^2R$  effects, whereas  $DC_{LLLF}$ , being a simpler linear formulation, neglects higher-order terms and therefore underperforms. Ultimately, when observing the  $AC_{SPF}$  results horizontally for each case, the  $DC_{LQCP}$  was revealed to generalize better and be more consistent with violation reduction, at scale.  $DC_{LLOA}$  did have the lowest violations sparingly compared to the others, but performed poorly at scale (e.g., for `case_13659` in  $AC_{SPF}$ , complete AC feasibility was achieved in  $DC_{LQCP}$ , with  $DC_{LLOA}$  recording violations closer to the linearized  $DC_{LLLF}$ .

**2) Bar Graph Sensitivity Analysis:** Following the realization of  $DC_{LQCP}$ 's better generalizable performance, imperative sensitivity analysis was conducted. Fig. 3 provides a visual reflection of the numerical trends, presenting the *sum of violation magnitudes* across all buses, branches, and limits. Unlike Tables I-II, which details violation *counts* and *maxima*, these plots capture the aggregate severity. The top panels correspond to  $DC_{BASE} \rightarrow AC$  pipelines, while the bottom panels use lossy  $DC_{LQCP}$  initializations. Across most test systems, the distributed-slack  $AC_{SPF}$  reconciliation yields the lowest summed violations in every category. From the upper plots, moving from  $AC_{BASE}$  to  $AC_{SPF}$  reduces both active- and reactive-power violation magnitudes by roughly *four orders of magnitude* (from  $10^{-3}$ – $10^2$ , down to  $10^{-4}$ – $10^{-3}$  p.u.). The same trend extends to voltage and thermal violations, which remain low under  $AC_{SPF}$ . In contrast,  $AC_{BTS}$  and  $AC_{BASE}$  show higher aggregate magnitudes.  $AC_{DS}$  performed well in active power and voltage violation reduction, but performed poorly in reducing reactive power and thermal violations.

Comparing the upper and lower rows, lossy initializations ( $DC_{LQCP}$ ) further reduce total violation magnitudes by an additional one-to-two orders of magnitude across all AC types.

The  $DC_{LQCP}$  formulation captures loss and angle effects more accurately than  $DC_{BASE}$ , producing better-aligned initializations and greater AC feasibility. Consequently, the  $DC_{LQCP} \rightarrow AC_{SPF}$  pipeline is the most consistent at violation reduction across test cases. These plots reinforce the trends in Tables I-II: incorporating lossy DC models and distributed slack improves both constraint satisfaction and numerical stability.

#### B. Key Metrics for ACPF Variants Assessment

The following study gives a extensive comparative analysis of the ACPF variants from Section II. After demonstrating that  $DC_{LQCP} \rightarrow AC_{SPF}$  reduces violations and often fully restores AC feasibility, further performance analysis is required.

**1) Performance Metrics Table:** Table III summarizes key performance metrics for 10 core test cases, comparing cost deviation, mean absolute error, iteration behavior, and solving time across all ACPF variants. Clear trends show that distributed-slack formulations,  $AC_{DS}$  and  $AC_{SPF}$ , yield the lowest cost deviation and error magnitudes through improved active-power balancing. Cost differences drop by up to 93% relative to  $AC_{BASE}$ , while mean absolute errors approach zero for most systems (e.g.,  $AC_{SPF}$  maintains  $\leq 0.05$  p.u.). Iteration metrics reflect the effects of tolerance-based PV/PQ switching: both  $AC_{BTS}$  and  $AC_{SPF}$  reach zero reactive power violations, though  $AC_{SPF}$  consistently converges faster—reducing total iterations by about 50% in `case_2869`. In contrast,  $AC_{BASE}$  and  $AC_{DS}$  complete in a single recalculation loop but require longer inner iterations, at times. Full feasibility was not restored only for `case_2000`, likely due to high line impedance ratios ( $r/x$ ) limiting reactive controllability. As feasibility restoration is the pipeline's focus, convergence rate was not prioritized, though future work will address it [24]. Solving times align with iteration behavior: smaller systems (e.g., `case_89`,

TABLE III: PERFORMANCE METRICS IN BASE CASE DCOPF FOR ACPF VARIANTS ACROSS MULTIPLE TEST CASES

Test case	Cost Difference (%)					Mean Absolute Error (p.u.)					Iteration Count (Total)				Solving Time (s)	
	AC <sub>BASE</sub>	AC <sub>BTS</sub>	AC <sub>DS</sub>	AC <sub>SPF</sub>	Improv. (%)	AC <sub>BASE</sub>	AC <sub>BTS</sub>	AC <sub>DS</sub>	AC <sub>SPF</sub>	Improv. (%)	AC <sub>BASE</sub>	AC <sub>BTS</sub>	AC <sub>DS</sub>	AC <sub>SPF</sub>	ACOPF	AC <sub>SPF</sub>
case_30	1.21	1.71	0.36	0.32	(74, 81, 11)	0.00	0.02	0.01	0.00	(0, 100, 100)	4	19	4	3	1.79	0.21
case_39	1.38	1.43	0.30	0.26	(81, 82, 13)	0.01	0.03	0.01	0.00	(100, 100, 100)	3	20	3	8	0.41	0.13
case_89	0.33	0.36	0.19	0.20	(39, 44, -5)	0.02	0.04	0.02	0.00	(100, 100, 100)	4	42	4	12	0.42	0.23
case_118	2.19	2.82	0.24	0.18	(92, 94, 25)	0.01	0.04	0.00	0.01	(0, 75, -100)	4	60	3	18	0.19	0.22
case_1354	0.41	0.58	0.12	0.28	(32, 52, -133)	0.01	0.05	0.03	0.02	(0, 60, 33)	4	357	3	152	2.78	64.10
case_2000 <sup>o</sup>	2.11	2.14	0.91	0.82	(61, 62, 10)	0.23	0.20	0.02	0.05	(78, 75, -150)	3	208	4	81	3.24	36.10
case_2869	0.54	0.62	0.31	0.37	(31, 40, -19)	0.04	0.14	0.03	0.04	(0, 71, -33)	4	777	3	380	4.88	187
case_6468	1.65	1.89	0.26	0.24	(85, 87, 8)	0.07	0.12	0.04	0.05	(29, 58, -25)	4	3396	4	1670	59.05	2213
case_9241	1.60	1.11	0.21	0.20	(88, 82, 5)	0.02	0.13	0.02	0.02	(0, 85, 0)	3	2204	3	1356	30.18	6104
case_13659	1.81	1.31	0.15	0.13	(93, 90, 13)	0.01	0.04	0.01	0.01	(0, 75, 0)	4	6452	3	3320	127.14	7170

\* AC variants have higher iteration counts due to PV/PQ switching. <sup>o</sup> case\_2000 incurred violations of inequality constraints.

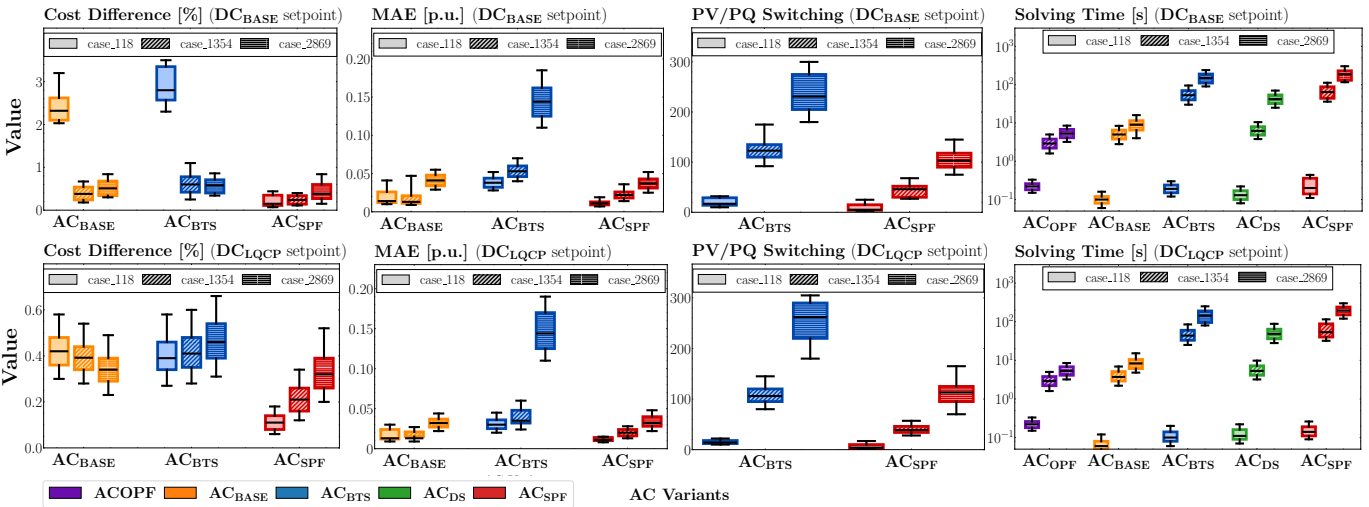


Fig. 4: Boxplot comparison of different AC variants' metrics across test cases: case\_118, case\_1354, and case\_2869 (with mean and min–max extremes). The AC variants shown have different DC setpoints: (top) DC<sub>BASE</sub> and (bottom) DC<sub>LQCP</sub>. The plots are taken over load uncertainty with  $\sigma = 15\%$ , for 1000 samples per case. Metrics shown (left to right): cost difference, mean absolute error, iteration count, and solving time. Results are reported for AC<sub>OPF</sub> (purple), AC<sub>BASE</sub> (orange), AC<sub>BTS</sub> (blue), AC<sub>DS</sub> (green), and AC<sub>SPF</sub> (red).

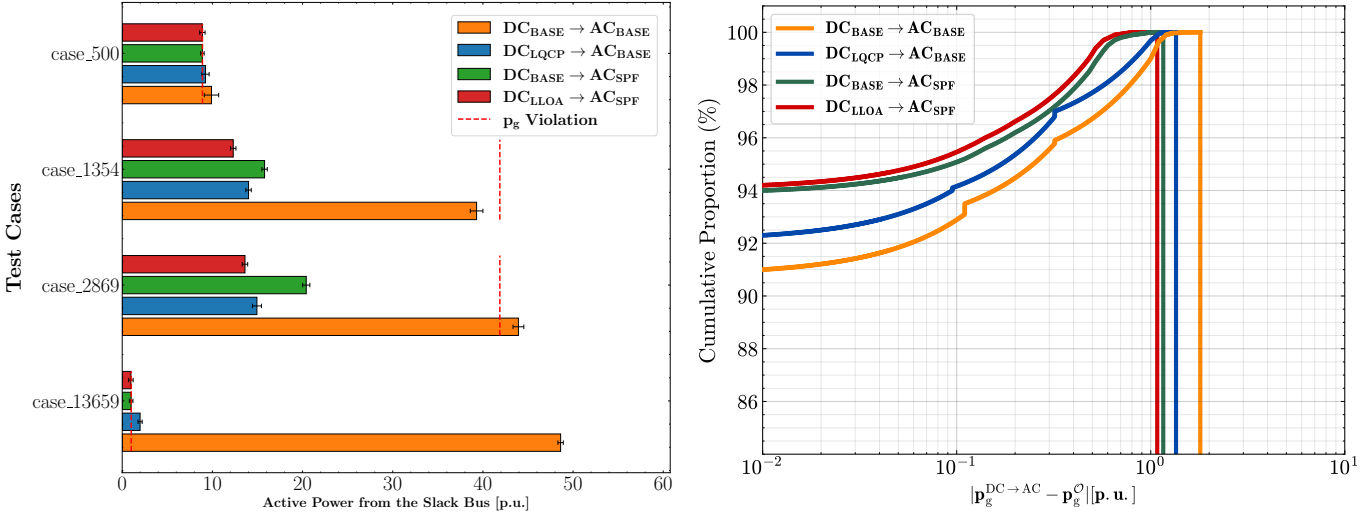
case\_118) run comparably or slightly faster under AC<sub>SPF</sub>, while larger networks slow down due to iterative refinement. Still, the gains in cost and feasibility confirm AC<sub>SPF</sub> has a good balance between accuracy and computational efficiency.

2) *Box Plot Sensitivity Analysis:* Fig. 4 illustrates the statistical distribution of performance metrics for three cases, revealing the robustness and variability of each ACPF variant. The upper plots correspond to DC<sub>BASE</sub> → AC pipelines, while the lower plots represent DC<sub>LQCP</sub> setpoints. The lossy DC generally yields a lower average cost difference and MAE, though with slightly higher variability across realizations. The DC<sub>LQCP</sub> initialization also reduces iteration counts and solving times—particularly for case\_118 and case\_1354—owing to its pre-accounting of power losses and generator redispatch. Since the AC reconciliation must only distribute the residual loss (i.e., remaining mismatch after DC loss approximation), convergence is faster. However, reactive-power control adjustments still dominate iteration requirements in larger networks. Across all metrics, AC<sub>SPF</sub> achieves the tightest distributions with the lowest mean values for both cost difference and MAE. The reduced interquartile ranges in AC<sub>SPF</sub> indicate superior consistency and robustness. For iteration count and solving time, AC<sub>SPF</sub> exhibits apparent higher computational effort, but remains competitive—with improved accuracy and reliability.

### C. Distributed Slack Effects on Active Power

The analysis examines distributed- versus single-slack-bus modeling in ACPF, isolating how DC and AC variants separately affect loss handling. It also evaluates whether DC models with higher degrees of freedom paired with simpler AC models (and vice versa) can yield acceptable performances.

1) *Bar Plot Sensitivity Analysis:* The horizontal bar plots in Fig. 5(a) reveal significant differences in slack-bus active-power requirements across four pipeline combinations. The red and green pipelines using AC<sub>SPF</sub> consistently yield active-power violations below  $10^{-3}$  p.u. Among them, DC<sub>LLOA</sub> → AC<sub>SPF</sub> produces the smallest active-power changes across all test cases. This behavior arises from the distributed-slack mechanism, which shares losses in proportion to generator reserve capability, rather than a single slack bus. By contrast, DC<sub>BASE</sub> → AC<sub>BASE</sub> exhibits the largest slack-bus injections, since a single slack must absorb losses after a lossless DCOPF—pushing loss accountability to that unit. The pipeline DC<sub>LQCP</sub> → AC<sub>BASE</sub> also employs a single slack, but its setpoints originate from a DCOPF that accounts for losses, yielding a notable reduction relative to DC<sub>BASE</sub>. Consequently, using DC<sub>LQCP</sub> or DC<sub>LLOA</sub> improves AC reconciliation compared with DC<sub>BASE</sub> (seen in the reduction from orange to blue, and green to red). With low perturbations of  $\sigma = 5\%$ , single-slack pipelines may converge



(a) Active power from the slack-bus (mean with min–max error bars)

Fig. 5: Pipeline comparison across different DC and AC variants, over load uncertainty with  $\sigma = 5\%$ . (a) Slack-bus active power using 100 per case, for: case\_500, case\_1354, case\_2869, and case\_13659 under DC<sub>BASE</sub> → AC<sub>BASE</sub> (orange), DC<sub>LQCP</sub> → AC<sub>BASE</sub> (blue), DC<sub>BASE</sub> → AC<sub>SPF</sub> (green), and DC<sub>LLOA</sub> → AC<sub>SPF</sub> (red). Dashed (red) line is the active power violation. (b) Cumulative density factor (CDF) plot of unit-wise active-power deviation  $|p_g^{\text{DC} \rightarrow \text{AC}} - p_g^{\mathcal{O}}|$  across generators in case\_1354, using 1000 per case, with an x-axis log-scale.

without active-power violations, yet the slack generator remains stressed, underscoring its inherent fragility.

2) *Cumulative Density Function Analysis:* Fig. 5(b) compares  $|p_g^{\text{DC} \rightarrow \text{AC}} - p_g^{\mathcal{O}}|$  (p.u.) across pipelines on a logarithmic scale. The two distributed-slack recoveries, DC<sub>LLOA</sub> → AC<sub>SPF</sub> and DC<sub>BASE</sub> → AC<sub>SPF</sub>, dominate: for any error threshold, their curves lie above the single-slack ones, indicating fewer large generator-setpoint deviations. At  $10^{-2}$  p.u., about 94.5%, 94%, 92.3%, and 91% of generators lie below this error for the four pipelines, respectively. A notch near  $10^{-1}$  p.u. on the AC<sub>BASE</sub> curves reflects loss aggregation under a single slack, producing a cluster of similar deviations. The right tails confirm the same ordering: AC<sub>SPF</sub> pipelines saturate near 1 p.u., whereas AC<sub>BASE</sub> ones require larger errors ( $\sim 1.2\text{--}1.3$  p.u.) to reach 100%. These results underscore the advantage of distributed slack and advanced AC recovery in minimizing generator output errors and mitigating the limitations of single-slack aggregation.

#### D. Bus-type Switching Effects on Voltage and Reactive Power

As discussed in Section II-B, reactive power and voltage are tightly coupled in ACPF. Fig. 6 shows this relationship across five test cases under load uncertainty  $\sigma = 5\%$ . The upper box plots show voltage magnitudes with dashed limits, while the lower plots depict mean reactive violations. AC<sub>BTS</sub> eliminates most reactive violations through dynamic PV/PQ switching, maintaining feasibility but causing larger voltage deviations—particularly in case\_1354 and case\_2869, where voltages approach their upper limits. While voltage–reactive coupling allows PV/PQ switching to restore most voltage setpoints, near-limit voltages may demand reactive support beyond generator capability, leading to increased violations. AC<sub>BASE</sub> enforces setpoints rigidly, yielding more reactive-limit breaches, whereas loss-aware DC<sub>LQCP</sub> and DC<sub>LLOA</sub> pre-account for losses and phase angles, reducing voltage deviations

and violations. Among DC variants, DC<sub>LQCP</sub> best maintained voltages within limits, even with AC<sub>BASE</sub>. Overall, AC<sub>BTS</sub> demonstrates the benefits of reactive flexibility, while lossy DC pipelines help keep bus voltages near nominal values. These results highlight the voltage–reactive trade-off in AC feasibility recovery and the value of loss-aware setpoints for balanced operation. Voltage initializations from AC<sub>BASE</sub> also improved convergence and reduced violations relative to a flat start.

## IV. CONCLUSION

This paper investigates AC feasibility restoration pipelines for DCOPF dispatches. A comprehensive empirical study is conducted, applying various DCOPF and ACPF variants. The most effective and consistent pipeline for restoring AC feasibility from DC solutions is found to be DC<sub>LQCP</sub> → AC<sub>SPF</sub>. The results show that integrating a structured ACPF—featuring distributed slack and reactive power limited generators—with loss-augmented DCOPF dispatches, can yield ACOPF feasible outcomes. This workflow reduces violations in active power, voltage, reactive power, and thermal limits while lowering the cost difference. For reference, applying the structured pipeline to the 13,659-bus case achieved improvements of 93% in cost difference, 75% in mean absolute error, and an improved convergence rate compared to single-slack methods. The link between voltage and reactive power violations is also examined. Future work will focus on improving the pipeline’s computational efficiency, with a promising direction being the integration of parameterized DCOPF and structured ACPF in an end-to-end self-supervised learning framework to enhance AC feasibility, and scalability for DC-operated markets.

## REFERENCES

- [1] H. Kile, K. Uhlen, L. Warland, and G. Kjølle, “A comparison of AC and DC power flow models for contingency and reliability analysis,” in *18th Power Systems Computation Conference (PSCC)*, Poland, 2014.

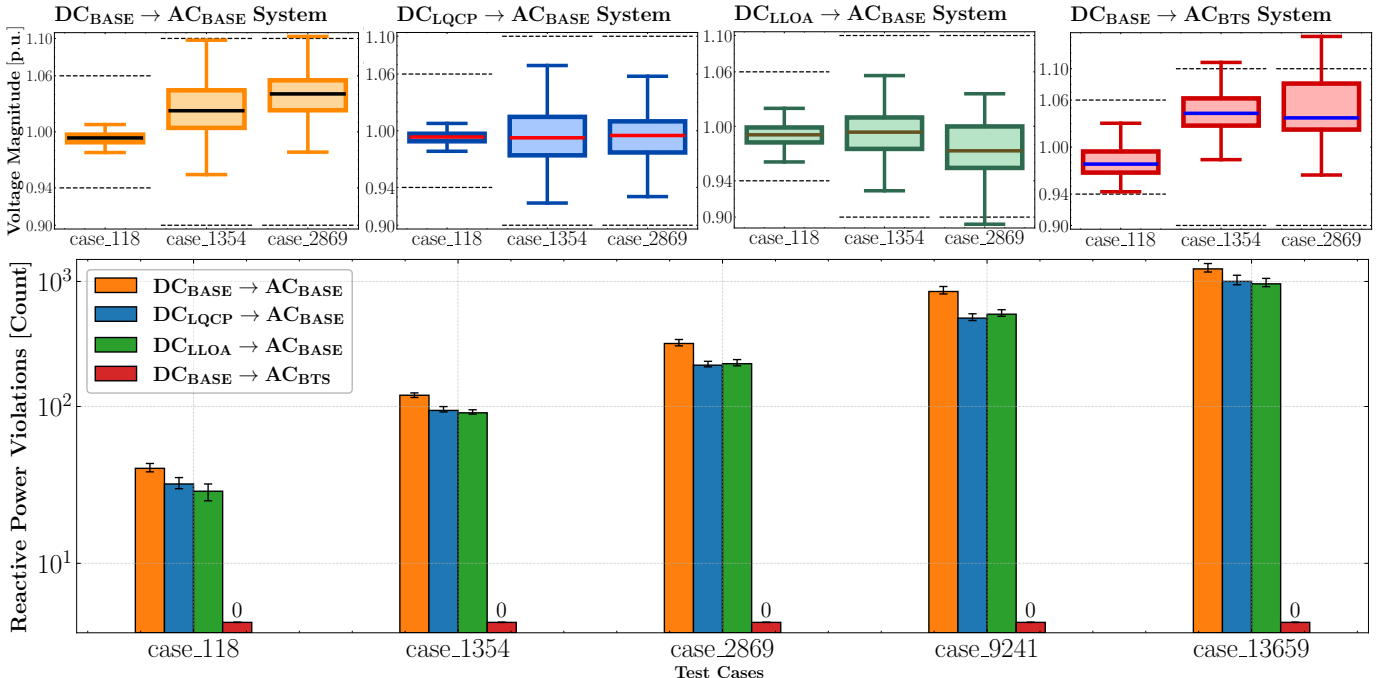


Fig. 6: Interplay between voltage magnitude and reactive power for various pipelines. The plots are taken over load uncertainty with  $\sigma = 5\%$ , for 1000 samples per case. The top box plots (mean with min–max extremes) show the voltage distributions for three cases (case\_118, case\_1354, and case\_2869). Dashed lines are voltage limits. The bottom plots show mean reactive power violations (with min–max error bars), with a y-axis log-scale, using: DC<sub>BASE</sub> → AC<sub>BASE</sub> (orange), DC<sub>LQCP</sub> → AC<sub>BASE</sub> (blue), DC<sub>LLOA</sub> → AC<sub>BASE</sub> (green), and DC<sub>BASE</sub> → AC<sub>BTS</sub> (red).

- [2] M. Liu and G. Gross, "Effectiveness of the distribution factor approximations used in congestion modeling," in *14th Power Systems Computation Conference (PSCC)*, Seville, Spain, June 2002.
- [3] T. J. Overbye, X. Cheng, and Y. Sun, "A comparison of the AC and DC power flow models for LMP calculations," in *37th Hawaii International Conference on System Sciences (HICSS)*, January 2004.
- [4] K. Purchala, L. Meeus, D. Van Dommelen, and R. Belmans, "Usefulness of DC power flow for active power flow analysis," in *IEEE Power & Energy Society General Meeting*, June 2005, pp. 454–459.
- [5] F. Li and R. Bo, "DCOPF-based LMP simulation: Algorithm, comparison with ACOPF, and sensitivity," *IEEE Transactions on Power Systems*, vol. 22, no. 4, pp. 1475–1485, November 2007.
- [6] B. Stott, J. Jardim, and O. Alsaç, "DC power flow revisited," *IEEE Transactions on Power Systems*, vol. 24, no. 3, pp. 1290–1300, 2009.
- [7] Y. Qi, D. Shi, and D. Tylavsky, "Impact of assumptions on DC power flow model accuracy," in *North American Power Symposium (NAPS)*, September 2012.
- [8] B. Taheri and D. K. Molzahn, "Optimizing parameters of the DC power flow," vol. 235, no. 110719, October 2024, presented at the 23rd Power Systems Computation Conference (PSCC).
- [9] C. Coffrin, P. Van Hentenryck, and R. Bent, "Accurate load and generation scheduling for linearized DC models with contingencies," in *IEEE Power & Energy Society General Meeting*, July 2012.
- [10] H. Cetinay, S. Soltan, F. A. Kuipers, G. Zussman, and P. Van Mieghem, "Comparing the effects of failures in power grids under the AC and DC power flow models," *IEEE Transactions on Network Science and Engineering*, vol. 5, no. 4, pp. 301–312, October 2018.
- [11] R. Kaye and F. F. Wu, "Analysis of linearized decoupled power flow approximations for steady-state security assessment," *IEEE Transactions on Circuits and Systems*, vol. 31, no. 7, pp. 623–636, July 1984.
- [12] S. Bolognani and S. Zampieri, "On the existence and linear approximation of the power flow solution in power distribution networks," *IEEE Transactions on Power Systems*, vol. 31, no. 1, pp. 163–172, 2016.
- [13] K. Dvijotham and D. K. Molzahn, "Error bounds on the DC power flow approximation: A convex relaxation approach," in *55th IEEE Conference on Decision and Control (CDC)*, 2016, pp. 2411–2418.
- [14] K. Baker, "Solutions of DC OPF are never AC feasible," in *ACM e-Energy*, 2021.
- [15] A. Zamzam and K. Baker, "Learning optimal solutions for extremely fast ACOPF," in *IEEE SmartGridComm*, 2020.
- [16] H. Zhao, M. Tanneau, and P. Van Hentenryck, "A linear outer approximation of line losses for DC-based optimal power flow problems," *Electric Power Systems Research*, vol. 212, p. 108272, 2022, presented at the 22nd Power Systems Computation Conference (PSCC).
- [17] A. Agarwal, A. Pandey, M. Jereminov, and L. Pileggi, "Continuously differentiable analytical models for implicit control within power flow," *arXiv:1811.02000*, Nov. 2018.
- [18] X. Fang, Z. Yang, J. Yu, and Y. Wang, "AC feasibility restoration in market clearing: Problem formulation and improvement," *IEEE Transactions on Industrial Informatics*, vol. 18, no. 11, 2022.
- [19] B. Taheri and D. K. Molzahn, "AC power flow feasibility restoration via a state estimation-based post-processing algorithm," *Electric Power Systems Research*, vol. 235, no. 110642, Oct. 2024, presented at the 23rd Power Systems Computation Conference (PSCC).
- [20] C. Coffrin, P. Van Hentenryck, and R. Bent, "Approximating line losses and apparent power in AC power flow linearizations," in *IEEE Power and Energy Society General Meeting*, 2012.
- [21] A. J. Wood and B. F. Wollenberg, *Power Generation, Operation, and Control*, 2nd ed. New York: Wiley, 1996.
- [22] V. N. Bharatwaj, A. R. Abhyankar, and P. R. Bijwe, "Iterative DCOPF model using distributed slack bus," in *IEEE Power and Energy Society General Meeting*, 2012.
- [23] J. Zhao, H. Chiang, P. Ju, and H. Li, "On PV–PQ bus type switching logic in power flow computation," in *16th Power Systems Computation Conference (PSCC)*, Glasgow, Scotland, UK, 2008.
- [24] L. Zeng, H.-D. Chiang, L. S. Neves, and L. F. C. Alberto, "On the accuracy of power flow and load margin calculation caused by incorrect logical PV/PQ switching: Analytics and improved methods," *International Journal of Electrical Power & Energy Systems*, vol. 147, 2023.
- [25] R. D. Zimmerman, C. E. Murillo-Sánchez, and R. J. Thomas, "Matpower: Steady-state operations, planning, and analysis tools for power systems research and education," *IEEE Transactions on Power Systems*, vol. 26, no. 1, pp. 12–19, 2011.
- [26] C. Coffrin, R. Bent, K. Sundar, Y. Ng, and H. Wang, "PowerModels.jl: An open-source framework for exploring power flow formulations," in *20th Power Systems Computation Conference (PSCC)*, 2018.
- [27] L. Thurner, A. Scheidler, F. Schäfer, J.-H. Menke, J. Dollichon, F. Meier, and J. M. Myrzik, "pandapower—An open-source Python tool for convenient modeling, analysis, and optimization of electric power systems," *IEEE Transactions on Power Systems*, vol. 33, p. 6510, 2018.